

Extended Object Tracking With Transparency Mitigation

Tobias Hirscher, Hanne Hettmann, Marco Heimberger, und Jens Honer *

Zusammenfassung: We propose an efficient approach to enhance the measurement likelihood of differentiable star-convex extended target models to mitigate unlikely association processes due to self-occlusion. Our approach allows us to retain an efficient computation of likelihoods and hence the correction step for extended targets while simultaneously penalizing unlikely measurement to target associations. In combination with a filter that is able to process multi-modal distributions we find that this leads to a significant increase in tracking performance, in particular during the initialization of the filter. We demonstrate an implementation based on the recently proposed Gaussian process extended target model and show how our redefined likelihood improves real-world tracking performance using automotive LIDAR data.

Schlüsselwörter: extended target, Gaussian process, transparency

1 Introduction

Robust automotive environment perception is based to a large extent on the tracking of dynamic targets. For this purpose, the recorded data from one or several sensors is processed to continuously estimate the pose and behavior of an unknown number of objects in the vehicle surrounding. Due to the high resolution of modern sensors like laser scanners a single target potentially generates more than one measurement per scan. To track such an extended target the simple point object model commonly used in literature has to be replaced by a more advanced model of the target object [1].

The widely used approach of adding a preprocessing step to reduce the complex measurements patterns to trackable features of the extended targets [2] results in using heuristics and a loss of information. The spatial distribution model avoids this problem by removing the preprocessing step and working on the full set of measurements [3]. [4] introduced the random matrices model that assumes the object extent is the primary source of measurement uncertainty. For Gaussian distributed measurements they provide a closed form expression for the target state distribution in the form of an inverse Wishart distribution coupled with a Gaussian distributed kinematic state. The restriction of negligible measurement uncertainty was later generalized by [5], with further improvements of this model done by [6] and [7]. [8] suggests rectangular and elliptical shapes by means of superposition of Gaussian likelihoods, whereas [9] describes a particle filter for tracking rectangular shapes. An approach to track general star-convex shapes was proposed by [10, 11] in the

*Valeo Schalter und Sensoren GmbH, 74321 Bietigheim-Bissingen, Germany (e-mail: {tobias.hirscher, hanne.hettmann, marco.heimberger, jens.honer}@valeo.com).

form of the random hypersurface model. [12] provide a filter to track arbitrary forms by employing local grid maps.

The technique to illustrate the boundary of extended objects described in the present paper was initially applied in the context of a tracking application in [13]. Due to its analytical properties, the Gaussian processes (GP) have often been utilized in the fields of machine learning, signal processing and statistics. They can be regarded as distribution of functions and in turn allow the representation of an object contour as star-convex shape described by a radial function. Coupled with a multivariate Gaussian to represent the distribution of the kinematic state [13] could track arbitrary star-convex targets while simultaneously estimate their shape.

The original definition of GPs is not applicable for recursive application like object tracking since the different measurements are recorded sequentially in each measurement cycle. For this reason, [14] used the recursive formalism of the GPs introduced in [13]. That this measurement model can be used within a modern multi-object tracking framework to track multiple objects with different kind of shapes was shown in [15].

A major weakness of the GP measurement model implemented in [13] and [15] is the fact that the correction step is not unique but various combinations of the objects center of rotation and its boundary contour exist in parallel. Consequently, there is a chance of associating measurements to the wrong, i.e. the occluded side of the shape, which implicitly leads to the assumption of a transparent target. In the present paper we suggest a solution for the described transparency problem and demonstrate the results with real-word data recorded with a state of the art automotive laser scanner.

The paper is structured as follows. First we are providing the main idea of Gaussian processes and how they can be fitted into tracking applications in section 2.2. Then we present how the single object is modeled and how the corresponding Gaussian process measurement model is executed in section 3. section 4 is pointing out the transparency mitigation and its use together with the Gaussian Process measurement model. Numerical results on experimental data is shown in section 5. Finally the paper is concluded in section 6.

2 Target Motion and Measurement Model

The following section imparts the basic knowledge about Gaussian processes and explains how they can be used to model extended objects in the context of tracking applications. In this paper scalars are stated with lower case letters (e.g. x), vectors with bold printed lower case letters (e.g. \mathbf{x}) and both sets and matrices with upper case letters (e.g. X).

2.1 Recursive Gaussian Process

A GP [16] is a stochastic process which can be regarded as multivariate Gaussian distribution over functions. It can be described with

$$f(\mathbf{u}) \sim \mathcal{GP}(x(\mathbf{u}), k(\mathbf{u}, \mathbf{u}')) \quad (1)$$

and uniquely defined by its mean function and its covariance function

$$x(\mathbf{u}) = E[f(\mathbf{u})] \quad (2)$$

$$k(\mathbf{u}, \mathbf{u}') = E[(f(\mathbf{u}) - x(\mathbf{u}))(f(\mathbf{u}') - x(\mathbf{u}'))]. \quad (3)$$

According to its interpretation as multivariate Gaussian distribution, the function values $f(u)$ of a GP are evaluated at the positions of the set of inputs u and follow the Gaussian distribution curve.

$$\begin{bmatrix} f(u_1) \\ \vdots \\ f(u_n) \end{bmatrix} \sim \mathcal{N}(\mathbf{x}, K), \text{ with } \mathbf{x} = \begin{bmatrix} x(u_1) \\ \vdots \\ x(u_n) \end{bmatrix} \quad K = \begin{bmatrix} k(u_1, u_1) & \dots & k(u_1, u_n) \\ \vdots & \ddots & \vdots \\ k(u_n, u_1) & \dots & k(u_n, u_n) \end{bmatrix}. \quad (4a)$$

Classical GPs are designed as batch processes, i.e. all the input data is available from the start [16]. [13] applied the recursive formulation of GPs derived in [14] to come up with the sensor data sequentially arriving in each update step. By the definition of the GP recursion as state space model it is possible to use a Kalman filter to recursively correct the GP estimation based on newly available measurements. Within this process the measurement model for the shape $f(u)$ of an extended target is defined as

$$y_t = f(u_t) + w, \quad w \sim \mathcal{N}(0, R), \quad (5)$$

w being the normal distributed zero-mean measurement noise with its covariance R . The goal of the recursion is to estimate the approximation \mathbf{f}_t of the function $f(u)$ at a finite set of specific basis values \mathbf{u}^f . The so-called basic vectors \mathbf{f}_t located at basic points $\mathbf{u}^f \hat{=} \{u_i^f \mid i = 1, \dots, n\}$ are recursively estimated at the timesteps $t = 0, 1, \dots$. Set of measurements $\mathbf{z}_t \hat{=} \{z_{t,i} \mid i = 1, \dots, m\}$ at corresponding inputs $\mathbf{u}_t \hat{=} \{u_{t,i} \mid i = 1, \dots, m\}$ are observed for that. The positions and the number n of basic vectors are the same for all timesteps t . For better readability we will omit the time index t in most of the case and use it only if is needed for a better understanding. The basis vectors are a sparse representation of the GP. Assuming that the measurements \mathbf{z} and the function values \mathbf{f} are jointly Gaussian, [16] showed that the conditional posterior density is given by

$$p(\mathbf{f} \mid \mathbf{z}_{1:t}) = \mathcal{N}(\mathbf{f}; \mathbf{x}^f, P^f) \quad (6)$$

using the mean function values $\mathbf{x}^f = [x_1^f(u_1^f), \dots, x_n^f(u_n^f)]$ at the basis points \mathbf{u}^f and the process noise covariance P^f . Further assuming a measurement process as defined in (5) with $w \sim \mathcal{N}(\mathbf{0}, R)$, the conditional measurement likelihood function [16] is given by

$$p(\mathbf{z} \mid \mathbf{f}) = \mathcal{N}(\mathbf{z}; \mathbf{z}_+, R^f). \quad (7)$$

Here the predicted measurements are $\mathbf{z}_+ = H^f \mathbf{x}^f$, the observation model and the measurement noise are

$$H^f = K_{mf} K_{ff}^{-1} \quad (8a)$$

$$R^f = K_{mm} + R - K_{mf} K_{ff}^{-1} K_{fm}. \quad (8b)$$

Here we use the short hand notation $K_{mf} = K(\mathbf{u}, \mathbf{u}^f)$, $K_{mm} = \text{diag}[K(\mathbf{u}, \mathbf{u})]$, $K_{ff} = K(\mathbf{u}^f, \mathbf{u}^f)$ and $K_{fm} = K(\mathbf{u}^f, \mathbf{u})$ for the kernels of the GP. The whole process can be described in terms of Kalman prediction and correction equations as shown in [15].

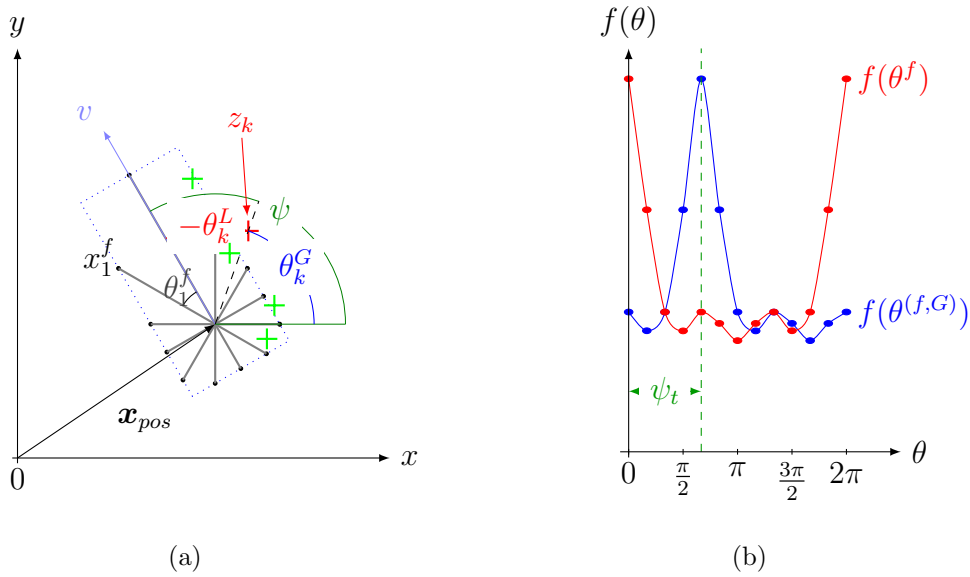


Abbildung 1: Gaussian process measurement model with its describing parameters. The approximation of a vehicle with basic vectors \mathbf{x}^f and the corresponding basic angles θ^f is visualize in (a). The green makes are examples of observations \mathbf{z} of a sensor while the red mark is a special marked observation showing the relation of local measurement angles θ^L to the velocity vector v and the orientation ψ of the object model. (b) illustrates the Gaussian process modeling the vehicle in (a) as function $f(\theta)$. The red line shows the smoothed local mean function $f(\theta^f)$ of the Gaussian process whereas the blue line is the function based on the global basic angles $\theta^{(f,G)}$.

2.2 Extended Object Model

Following the implementation described in [13], GPs can be applied to model moving extended objects with a radial shape. The basis points are defined at specific angles θ^f which span the interval $[0, 2\pi)$, whereas the values of the mean function \mathbf{x}^f describe the radial distance at the corresponding angles as illustrated in Fig. 1.

Augmenting the kinematic object model with the state space model of the GP, it is possible to simultaneously estimate the motion and the extent of an object. The combined state vector is then given by

$$\mathbf{x} = [(\mathbf{x}^{kin})^T \quad (\mathbf{x}^f)^T]^T, \quad \text{with} \quad \mathbf{x}^{kin} = [(\mathbf{x}_{pos})^T \quad \psi \quad (\mathbf{x}_{ho})^T]^T. \quad (9a)$$

The motion states \mathbf{x}^{kin} consist of the position $\mathbf{x}_{pos} = (x^c, y^c)$ and the target orientation ψ as well as the higher order components \mathbf{x}_{ho} of the center of rotation (COR) and the orientation ψ . In this work we are using only the velocity v of the COR as higher order component, therefore $\mathbf{x}_{ho} = v$. We also assume a constant target object shape, i.e. $\mathbf{x}^f = \mathbf{x}_0^f$. This assumption significantly decreases the computational effort of the correction step since it avoids the online inversion of the GP correlation kernel. Note that discrete changes between different shapes may be introduced by the use of a mixture model in combination with state transitions. The state vector and its covariance P are recursively predicted with an unscented transform (UT) similar to the one shown in [17] and corrected with an extended Kalman filter (EKF) in analogy to [13].

2.3 Covariance Function

The choice of the GP kernel or covariance function has a strong impact on the behaviour of the target shape. [13] used a periodic covariance function given by

$$k_{per}(\theta, \theta') = \sigma_f^2 e^{-\frac{2 \sin^2\left(\frac{|\theta-\theta'|}{2}\right)}{l^2}} + \sigma_r^2 \delta_{\theta\theta'}. \quad (10)$$

The parameter l denotes the length-scale which can be interpreted as the distance in the inputs required for a significant change in the outputs. The factor σ_f is the prior variance of the signal amplitude and σ_r is the variance of the Gaussian prior. Using a periodic kernel a GP can model 2π -periodic functions which allows different mean and covariance values at basis angles.

The symmetric covariance function also presented in [13] corresponds to the periodic covariance function with twice the frequency. It enables faster estimations of the object shape in case of centrally symmetric targets. Contrary to the periodic covariance function, the symmetric covariance function implies that the COR lies at the object's center. Since in the context of moving vehicles the COR is more likely to be at the center of the rear axis, [15] suggests an axis-symmetric covariance function.

Note that in the simplified case with constant target shape, i.e. $\mathbf{x}^f = \mathbf{x}_0^f$, additional symmetries within the GP kernel are not required.

3 Gaussian Process Tracking

In this section we will roughly describe the prediction step of the tracking filter and in more detail the combined measurement update of the kinematic state and the GP.

3.1 Target Prediction

The prediction of the GP state and covariance is carried out according to the equations of the GP in [15]. The prediction of the kinematic state is performed according to [17] via an UT implementation.

3.2 Measurement Correction

The a priori distribution of the state \mathbf{x} is recursively updated with a set of measurements $Z \hat{=} \{\mathbf{z}_k \mid k = 1, \dots, m\}$ at each timestep t .

In turn every measurement \mathbf{z} has to be associated with a local angle θ relative to the COR \mathbf{x}_{pos} and the orientation ψ of the object. These local angles are determined by

$$\boldsymbol{\theta}^L = \boldsymbol{\theta}^L(\mathbf{x}_{pos}, \psi) = \boldsymbol{\theta}^G(\mathbf{x}_{pos}) - \psi \quad (11)$$

with $\boldsymbol{\theta}^G(\mathbf{x}_{pos})$ the global angles of the measurements relative to the x-axis. This measurement process is depicted in Fig. 1. The local angles are used to describe the relation between the object states and the measurements

$$Y = \mathbf{x}_{pos} + p(\mathbf{x}_{pos})f(\boldsymbol{\theta}^L) + w \quad (12)$$

with w the measurement noise as defined in (5). The radial function $f(\cdot)$ describes the extent of the objects relative to \mathbf{x}_{pos} depending on the local angles $\boldsymbol{\theta}^L$. Last, the vector

$$\mathbf{p}_k(\mathbf{x}_{pos}) = \mathbf{p}(\boldsymbol{\theta}_k^G(\mathbf{x}_{pos})) = \begin{bmatrix} \cos(\boldsymbol{\theta}_k^G(\mathbf{x}_{pos})) \\ \sin(\boldsymbol{\theta}_k^G(\mathbf{x}_{pos})) \end{bmatrix} = \frac{\mathbf{z}_k - \mathbf{x}_{pos}}{\|\mathbf{z}_k - \mathbf{x}_{pos}\|} \quad (13)$$

is the unit vector from the target center in the direction of the respective measurement. By use of the above definitions (12) may be written as

$$Y = \mathbf{x}_{pos} + \mathbf{p}(\mathbf{x}_{pos})[H^f(\boldsymbol{\theta}^L)\mathbf{x}^f + \epsilon^f] + w, \quad \epsilon^f \sim \mathcal{N}(0, R^f(\boldsymbol{\theta}^L)) \quad (14)$$

$$Y = h(\mathbf{x}) + e, \quad e \sim \mathcal{N}(0, R_{gp}) \quad (15)$$

with the nonlinear measurement function

$$h(\mathbf{x}) = \mathbf{x}_{pos} + \mathbf{p}(\mathbf{x}_{pos})H^f(\boldsymbol{\theta}^L)\mathbf{x}^f, \quad (16)$$

and the combined measurement noise

$$R_{gp} = \mathbf{p}(\mathbf{x}_{pos})R^f(\boldsymbol{\theta}^L)\mathbf{p}(\mathbf{x}_{pos})^T + R. \quad (17)$$

Since R was already accounted in (17) it can be neglected in (8b). The combined likelihood of the kinematic state and the shape is in turn given by

$$p(Y | \mathbf{x}_+) = \mathcal{N}(Y; Z_+, R_{gp}) \quad \text{where} \quad Z_+ = h(\mathbf{x}_+). \quad (18)$$

The m measurements Z as well as the combined measurement noise R_{gp} and the nonlinear measurement function $h(\mathbf{x})$ are reformulated for the purpose of the correction step as

$$\mathbf{z} = [\mathbf{z}_1^T, \dots, \mathbf{z}_m^T]^T, \quad R_{gp} = \text{diag}[R_1, \dots, R_m], \quad h(\mathbf{x}) = [h_1(\mathbf{x})^T, \dots, h_m(\mathbf{x})^T]^T. \quad (19)$$

Using this augmented formulation, the a priori distribution of the state \mathbf{x} can be recursively updated by applying the EKF equations similar to [13] Following the well-known EKF formulation the nonlinearity of the measurement function $h(\mathbf{x})$ linearized and yields the Jacobian H . The assumption of a constant a priori known shape allows the analytical calculation (cp. [13]) of the gradient according to the following equations:

$$H = \frac{dh(\mathbf{x})}{d\mathbf{x}} = \frac{d}{d\mathbf{x}}[h_1(\mathbf{x})^T, \dots, h_n(\mathbf{x})^T]^T \quad (20)$$

$$\frac{d}{d\mathbf{x}}h_k(\mathbf{x}) = \left[\frac{dh_k(\mathbf{x})}{d\mathbf{x}_{pos}}, \frac{dh_k(\mathbf{x})}{d\psi}, \frac{dh_k(\mathbf{x})}{d\mathbf{x}_{ho}}, \frac{dh_k(\mathbf{x})}{d\mathbf{x}^f} \right]^T = \left[H_{pos}, \mathbf{h}_\psi, H_{ho}, H_{\mathbf{x}^f} \right]^T \quad (21)$$

with

$$\begin{aligned} \frac{dh_k(\mathbf{x})}{d\mathbf{x}_{pos}} &= \mathbf{I} + \frac{\partial p_k(\mathbf{w})}{\partial \mathbf{w}} \Big|_{\mathbf{w}=\mathbf{x}_{pos}} H^f(\boldsymbol{\theta}_k^L)\mathbf{x}^f + p_k(\mathbf{x}_{pos}) \frac{\partial H^f(u)}{\partial u} \Big|_{u=\boldsymbol{\theta}_k^L} \frac{\partial \boldsymbol{\theta}_k^G(\mathbf{w})}{\partial \mathbf{w}} \Big|_{\mathbf{w}=\mathbf{x}_{pos}} \mathbf{x}^f \\ \frac{dh_k(\mathbf{x})}{d\psi} &= -p_k(\mathbf{x}_{pos}) \frac{\partial H^f(u)}{\partial u} \Big|_{u=\boldsymbol{\theta}_k^L} \mathbf{x}^f \quad \frac{dh_k(\mathbf{x})}{d\mathbf{x}_{ho}} = \mathbf{0} \quad \frac{dh_k(\mathbf{x})}{d\mathbf{x}^f} = \mathbf{0} \end{aligned} \quad (22)$$

Note that the dimensions of above matrices are

$$H_{pos} \in \mathbb{R}^{2 \times 2}, \quad \mathbf{h}_\psi \in \mathbb{R}^{2 \times 1}, \quad H_{ho} \in \mathbf{0} \in \mathbb{R}^{2 \times (|\mathbf{x}^{kin}|-3)}, \quad H_{\mathbf{x}^f} \in \mathbb{R}^{2 \times |\mathbf{x}^f|}. \quad (23)$$

4 Transparency Mitigation

This section describes a modified likelihood function that penalizes associations of measurement to an unobservable part of the target model and represents the main contribution. The lack of such a penalty in the original Gaussian process target model [13] may lead to the association of measurements to the target surface opposite to the sensor-facing side and hence yield to wrong association between measurement and obstacle surface which leads in this regard to a false estimate of the COR. In the following we will use the term *transparent target* for this effect. The root cause of this behavior is the efficient association scheme within the Gaussian process target model in which the relative position of the measurement with respect to the center of the star-convex shape determines where on the surface the measurement point is assumed to originate, see eq. (16).

Since we do not want to compromise the efficiency of this approach we modify the likelihood function itself rather than the association logic according to

$$g(Z|\mathbf{x}) = g_f(Z|\mathbf{x})g_p(\gamma(Z, \mathbf{x})) \quad (24)$$

where $g_f(Z|\mathbf{x})$ is the association likelihood of the measurements Z to the track \mathbf{x} [18], with the weighting function $g_p(\gamma(Z, \mathbf{x}))$ depending on

$$\tilde{\gamma}(z, \mathbf{x}) = \frac{\left\langle \frac{dz}{d\theta^G}, \hat{z}(\mathbf{x}_{pos}) \right\rangle}{\left\| \frac{dz}{d\theta^G} \right\| \left\| \hat{z}(\mathbf{x}_{pos}) \right\|} \quad (25)$$

the angle between the tangential vectors of the curve given by (12) and its orthogonal projection on the tangential plane spanned by the field of view of the sensor. Note that this approach may be considered as a failure recognition of the association scheme. The modification will not create a better association between measurements and the target surface like in [19] but only determine its failure and in turn penalize such an association. In turn the approach should be combined with a sophisticated multi-hypothesis tracking framework like a Bernoulli Filter.

In order to decrease the complexity of our calculation we approximate

$$\gamma(z, \mathbf{x}) \approx \frac{\left\langle \frac{dz}{d\theta^G}, \mathbf{n}(\mathbf{x}_{pos}) \right\rangle}{\left\| \frac{dz}{d\theta^G} \right\| \left\| \mathbf{n}(\mathbf{x}_{pos}) \right\|} \quad (26)$$

in which we replaced $\hat{z}(\mathbf{x}_{pos})$ with $\mathbf{n}(\mathbf{x}_{pos})$ which is constant for a given target. This approximation is valid as long as field of view occupied by the target is small. This is usually the case for vehicles in front (or the rear) of the host vehicle and thus well justified for applications such as target tracking for adaptive cruise control. Note that in both cases the function γ only depends on the angle between the center of the target and the measurement point. The function $g_p(\gamma(Z, \mathbf{x}))$ is then chosen according to the specific sensor in use and the predominant use-cases. A simple but already sufficient realization of the function $\gamma(Z, \mathbf{x})$ for automotive LIDAR sensors and highway/rural road scenarios used to generate our results is illustrated in Fig. 2.

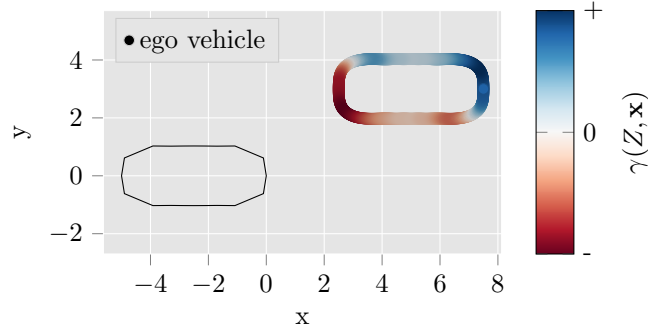
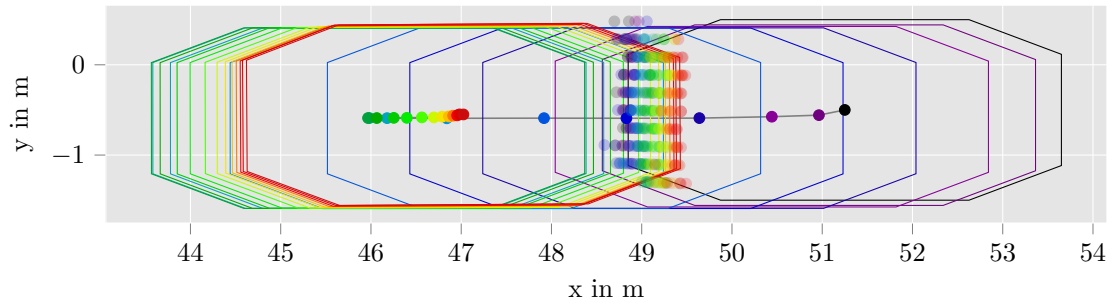
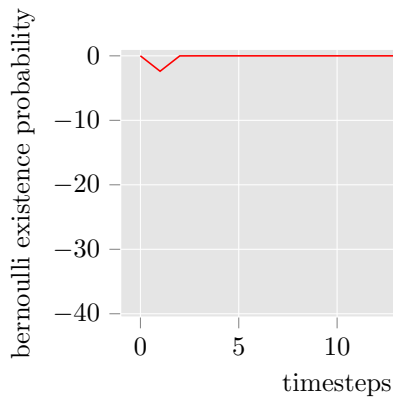


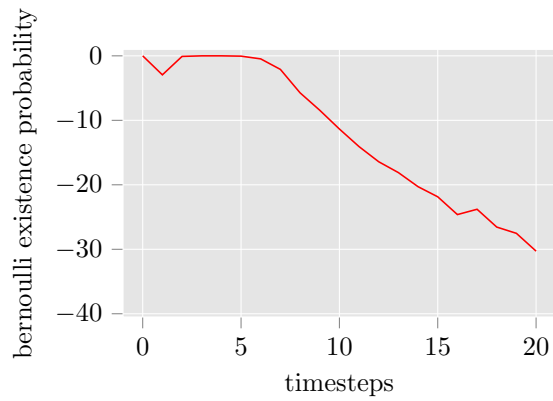
Abbildung 2: Schematic illustration of the visible part and the resulting $\gamma(Z, \mathbf{x})$. The black polygon is representing the ego vehicle from which the equally separated measurements shown as colored dots in the upper right are generated on the target surface. The intensity of $\gamma(Z, \mathbf{x})$ for each measurement is visualized with the colorbar on the right. The blue marks demonstrating observations which will get a penalty weight.



(a)



(b)



(c)

Abbildung 3: Second scenario to compare a Gaussian mixture target track with three components with and without applying the transparency weighting function $g_p(\gamma(Z, \mathbf{x}))$. The figure on the top visualizes the trajectory output of the bernoulli filter. On the bottom (b) is showing the logarithmic existence probability of the target track for every timestep with executing the weighting function and (c) without it.

5 Results

The effect of the transparency mitigation function $g_p(\gamma(Z, \mathbf{x}))$ we will evaluate in the following by evaluating two scenarios with real-world data. In the first scenario the observed

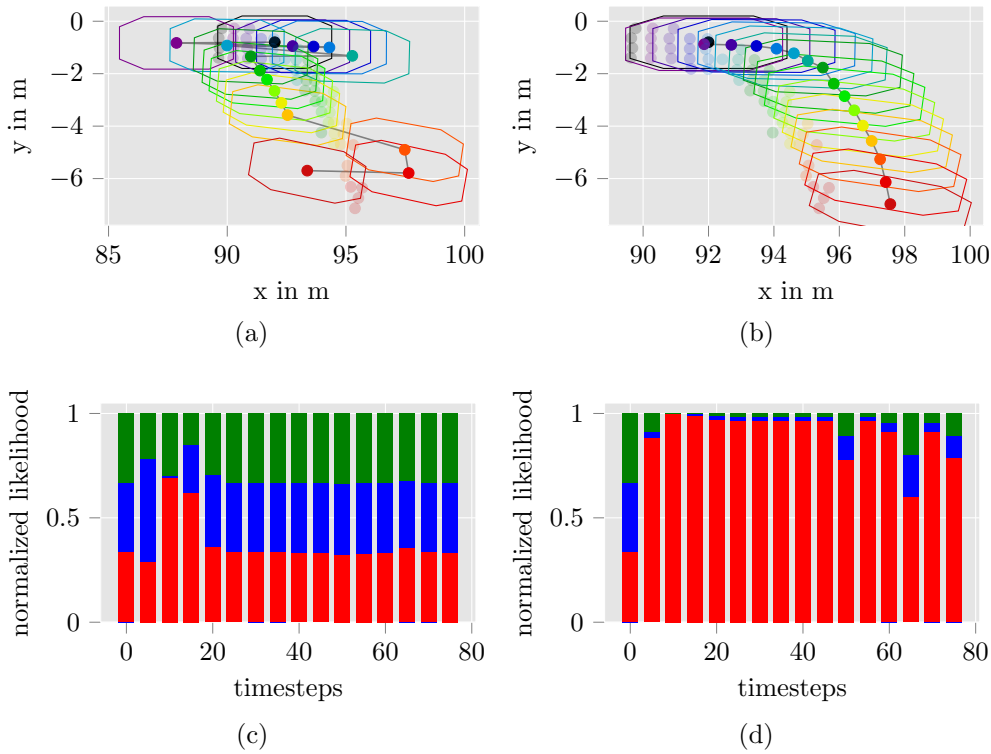


Abbildung 4: Comparison of a scenario with and without using the transparency weighting function $g_p(\gamma(Z, \mathbf{x}))$. In the top left the trajectory of a Gaussian mixture target track containing three components without applying the weighting function and in (b) with use of the function. In both figures (a) and (b) the measurements are shown with colored markers and the estimated target extent with colored polygons. The different painting illustrates the diverse timesteps. Black correspond to the initial step. Figure (c) as well as (d) are describing the normalized likelihoods of the three Gaussian mixture components at each timestep of the scenarios shown in (a) and (b).

target vehicle is driving in front of the host vehicle with a similar high velocity whereas in the second scenario the target vehicle is performing a right turn at approximately the same velocity as the host vehicle. The scenarios were recorded with a Valeo Scala Generation 1 LIDAR mounted in the front bumper of the host vehicle. The measurement frequency is 25 Hz and features a range of detection of 100 m for a target with 8% reflectivity and an azimuthal resolution of 0.25° in a field of view of $\pm 72.5^\circ$. All presented figures are visualized in the (right-handed) vehicle coordinate system with the origin located at the center of the rear axis of the host vehicle and the x -axis situated along the vehicle symmetry axis. For the target tracking framework we use a simple Bernoulli filter implementation [20]. The kinematic state of all components is modeled with (9a) and the target extent is modeled with a Gaussian Process with constant basic vectors $\mathbf{x}^f = \mathbf{x}_0^f$ and cardinality $|\mathbf{x}_0^f| = 20$. (see section 2.2.) The \mathbf{x}_0^f and corresponding angles are chosen to approximate a rectangular vehicle shape with a width and length of 2.0 m and 4.8 m, respectively. The covariance is provided by the correlation function (10) with parameters $\sigma_f = 0.30$ m, $\sigma_r = 0.06/4$ m and the lengthscale $l = \pi/10$. The noises parameters of the kinematic process are set to $\sigma_v = 1.55$ m/s² for the velocity and $\sigma_\phi = 0.22$ rad / s² for the yaw

rate. Last the measurement noise variance is chosen to be $R = 0.10\mathbf{I}$ m². To highlight the competition between different components in the Bernoulli filter we do not merge similar components. Since we always consider only a single measurement cluster this modification reduces the Bernoulli filter to a parallel implementation of different trackers with joint estimation of existence probability. We are using a simple weighting function

$$g_p(\gamma(Z, \mathbf{x})) = \prod_{i=1}^{|z|} f(\gamma(\mathbf{z}_i, \mathbf{x})) \quad \text{where} \quad f(\gamma(\mathbf{z}_i, \mathbf{x})) = e^{-\tilde{f}(\gamma(\mathbf{z}_i, \mathbf{x}))} \quad (27)$$

with

$$\tilde{f}(\gamma(\mathbf{z}_i, \mathbf{x})) = \begin{cases} \tau, & \text{if } \gamma(\mathbf{z}_i, \mathbf{x}) > 0 \\ 0, & \text{else} \end{cases}$$

to increase the effect of the transparency mitigation. In the following we will consider τ as penalty term for measurements on the transparent side of the measured object. Note that although the direction of travel of a target vehicle may be inferred from its shape with a single LIDAR measurement, the velocity and in particular its sign cannot. In turn there are two approaches to encode this ambiguity in the initialization: Either one initializes a single component with a single expected velocity and a high σ_v or one initializes the target track with several mixture components each using a different velocity. In the following we will show that in both case the transparency mitigation will improve the tracking performance.

5.1 Straight Driving Case

First we evaluate a scenario in which the target vehicle is driving in front of the host vehicle and the initial track velocity is set to $v = 0$ m/s. To compensate for the uncertainty of the initial velocity we choose a high variance $\sigma_v = 0.225$ m/s. The initial position $\mathbf{x}_{pos} = (51.25, -0.50)$ is chosen such that the Gaussian process contour aligns well with the measurements. Last the process noise is set to $\sigma_a = 1.55$ m/s². The results are shown in Fig. 3: Trajectories in Fig. 3a are constructed by extracting the component with the respective highest likelihood in every timestep. It can be clearly seen that the filter has difficulties adjusting to the correct velocity despite the relatively high process noise and needs several cycles to convergence to the correct velocity. Yet it is associating the measurement to the respective opposite side of the target model. The side that faces the sensor is not supported by measurements. If we now look at the (logarithmic) existence probability of the Bernoulli filter using the original implementation (Fig. 3b) of the likelihood does not indicate that the target is located in front of the measurements. In turn a filter will continue to track the target and most likely not recover. On the other hand our modified likelihood function (Fig. 3c) yields a steep drop in the existence probability and prevents such pathological behaviour.

5.2 Right Turn Case

In a right turn scenario we initialize the track as a multi-modal distribution with three likely but distinct velocities, namely $v_{1,2} = \pm 10$ m/s and $v_3 = 0$ m/s. The initial position

and orientation is set to $\mathbf{x}_{pos} = (92.0, -0.8)$ and yaw $\psi = 0$, i.e the same for all mixture components, and again chosen such that the Gaussian process contour is aligned with the measurements. Last, the process noise is set to $\sigma_a = 0.89$. Note that we are able to choose a lower variance due to the multi-modal initial state.

Fig. 4 shows the comparative output of the filter with (right) and without (left) taking into account the modified likelihood. The track trajectories in Fig. 4a and Fig. 4b are constructed in the same fashion as before (see Fig. 3a). The figures clearly show that without the modified likelihood the ambiguity between the components prevents a consistent estimation of the track: Since no component is dominant the track jumps between different components and creates the jagged trajectory. Moreover Fig. 4a shows the effect of the measurements being associated to the rear of the target, which, given the physical properties of the LIDAR, is highly unlikely. In contrast the modified likelihood prevents unlikely terms to contribute. (see Fig. 4d.) (Note that those components reappear after several steps. This is an artifact since we do not prune components which means we do not delete components with a low existence probability.

6 CONCLUSION

This paper presented an efficient approach to improve the likelihood function for extended targets to penalize unlikely association processes. We demonstrated the simple application of our approach on a Gaussian processes target model and provided examples of the effectiveness of our approach on real-world Lidar data recorded in typical driving situations.

Literatur

- [1] Y. Bar-Shalom, X. R. Li, and T. Kirubarajan, *Estimation with Applications to Tracking and Navigation: Theory Algorithms and Software*. Wiley, 2004.
- [2] C. Mertz, L. E. Navarro-Serment, R. MacLachlan, P. Rybski, A. Steinfeld, A. Suppe, C. Urmson, N. Vandapel, M. Hebert, C. Thorpe *et al.*, “Moving object detection with laser scanners,” *Journal of Field Robotics*, vol. 30, pp. 17–43, 2013.
- [3] K. Gilholm and D. Salmond, “Spatial distribution model for tracking extended objects,” *Radar, Sonar and Navigation, IEEE Proceedings*, vol. 152, no. 5, pp. 364–371, October 2005.
- [4] J. W. Koch, “Bayesian approach to extended object and cluster tracking using random matrices,” *IEEE Transactions on Aerospace and Electronic Systems*, vol. 44, no. 3, pp. 1042–1059, July 2008.
- [5] M. Feldmann, D. Franken, and W. Koch, “Tracking of extended objects and group targets using random matrices,” *IEEE Transactions on Signal Processing*, vol. 59, no. 4, pp. 1409–1420, April 2011.
- [6] M. Wieneke and W. Koch, “Probabilistic tracking of multiple extended targets using random matrices,” in *Signal and Data Processing of Small Targets*, O. E. Drummond, Ed. International Society for Optics and Photonics, 2010.

- [7] W. Koch and M. Feldmann, “Cluster tracking under kinematical constraints using random matrices,” *Robotics and Autonomous Systems*, vol. 57, no. 3, pp. 296–309, 2009.
- [8] K. Granström, C. Lundquist, and U. Orguner, “Tracking rectangular and elliptical extended targets using laser measurements,” in *in Proceedings of the 14th International Conference on Information Fusion (FUSION)*, July 2011.
- [9] A. Gning, B. Ristic, L. Mihaylova, and F. Abdallah, “Introduction to box particle filtering,” *IEEE Signal Processing Magazine*, 2012.
- [10] M. Baum and U. D. Hanebeck, “Random hypersurface models for extended object tracking,” in *IEEE International Symposium on Signal Processing and Information Technology (ISSPIT)*, Dec 2009, pp. 178–183.
- [11] —, “Extended object tracking with random hypersurface models,” *IEEE Transactions on Aerospace and Electronic Systems*, vol. 50, no. 1, pp. 149–159, January 2014.
- [12] M. Schütz, N. Appenrodt, J. Dickmann, and K. Dietmayer, “Simultaneous tracking and shape estimation with laser scanners,” in *16th International Conference on Information Fusion (FUSION)*. IEEE, 2013, pp. 885–891.
- [13] N. Wahlström and E. Özkan, “Extended target tracking using Gaussian processes,” *IEEE Transactions on Signal Processing*, vol. 63, no. 16, pp. 4165–4178, Aug. 2015.
- [14] M. F. Huber, “Recursive gaussian process regression,” in *IEEE International Conference on Acoustics, Speech and Signal Processing (ICASSP)*, May 2013, pp. 3362–3366.
- [15] T. Hirscher, A. Scheel, S. Reuter, and K. Dietmayer, “Multiple extended object tracking using gaussian processes,” in *19th International Conference on Information Fusion (FUSION)*. IEEE, 2016, pp. 868–875.
- [16] C. E. Rasmussen and C. K. I. Williams, *Gaussian Processes for Machine Learning*. MIT Press, 2006.
- [17] E. A. Wan and R. Van Der Merwe, “The unscented kalman filter for nonlinear estimation,” in *Adaptive Systems for Signal Processing, Communications, and Control Symposium 2000. AS-SPCC. The IEEE 2000*, 2000, pp. 153–158.
- [18] R. Altendorfer and S. Wirkert, “A complete derivation of the association log-likelihood distance for multi-object tracking,” *CoRR*, 2015.
- [19] F. Faion, A. Zea, M. Baum, and U. D. Hanebeck, “Partial likelihood for unbiased extended object tracking,” in *18th International Conference on Information Fusion (Fusion)*. IEEE, 2015, pp. 1022–1029.
- [20] R. P. S. Mahler, *Statistical Multisource-Multitarget Information Fusion*. Norwood, MA, USA: Artech House, Inc., 2007.